RSC Advances

PAPER

View Article Online
View Journal | View Issue

Cite this: *RSC Adv.*, 2021, **11**, 10986

A dual-functional nanovehicle with fluorescent tracking and its targeted killing effects on hepatocellular carcinoma cells

Xiaojie Zhang,†[ab] Qiming Gao,†[a] Qianfen Zhuang,†[b] Lu Zhang,†[c] Sihan Wang,[a] Libo Du,[b] Wenxi Yuan,[d] Caifang Wang,[d] Qiu Tian,[b] Hua Yu,[e] Yuming Zhao *[a] and Yang Liu[b]

All-in-one drug delivery nanovehicles with low cytotoxicity, high clinical imaging tracking capability, and targeted- and controlled-releasing performances are regarded as promising nanoplatforms for tumor theranostics. Recently, the design of these novel nanovehicles by low molecular weight amphiphilic chitosan (CS) was proposed. Based on fluorescent gold nanoclusters (AuNCs), a tumor-targeting nanovehicle (*i.e.* AuNCs-CS–AS1411) was prepared *via* electrostatic attraction between AuNC-conjugated chitosan (*i.e.* AuNCs-CS) and the anti-nucleolin aptamer, AS1411. After that, the anticancer drug methotrexate (MTX) was encapsulated into the nanovehicles and then the dual-functional nano-drug (*i.e.* MTX@AuNCs-CS–AS1411) was comparatively supplied to the human hepatocellular carcinoma cell line HepG2 and the human normal liver cell line LO2, to exhibit its "all in one" behavior. Under the conditions of the same concentration of MTX, MTX@AuNCs-CS–AS1411 demonstrates more intensive cytotoxicity and apoptosis-inducing activity against HepG2 cells than those against normal LO2 cells, mainly due to the targeting effect of AS1411 on the nucleolins that were found at high levels on the surface of tumor cells, but are at low levels or absent on normal cells. On the other hand, the MTX release from the MTX@AuNCs-CS–AS1411 was much faster in mildly acidic solution than that in neutral pH. Thus, it may provide a possibility to more significantly release MTX in intracellular lysosome of tumor cells, rather than let loose MTX during transport of the drug from blood vessels to tumor tissue. In conclusion, our dual-functional nanovehicle possesses high fluorescence efficiency and photostability, low cytotoxicity, pH-dependent controlled release, high sensitivity and target-specificity to cancer cells which allowed concurrent targeted imaging and delivery in cancer chemotherapies.

Received 14th December 2020
Accepted 8th March 2021

DOI: 10.1039/d0ra10486h

rsc.li/rsc-advances

Introduction

Hepatocellular carcinoma (HCC) is one of the leading causes of cancer-related deaths worldwide.[1,2] In each year, more than 600 000 people died of HCC.[3] Chemotherapy is one classic intervention for anti-cancer therapy. However, many anti-cancer drugs are poorly water-soluble, unspecific to healthy tissues which cause their low bioavailability and severe side-effects, including pain sores in the throat, nausea and vomiting and blood disorders.[4]

Recently, the design of targeted nanovehicles for drug delivery has provided an alternative approach in cancer chemotherapies. On one hand, it can elongate blood circulation time and improve the bioavailability of the hydrophobic drug inside tumour cells by using drug-encapsulated nanoparticles. On the other hand, it can facilitate tumour drug delivery by conjugating drug-encapsulated nanoparticles with targeting ligands.[5,6] These nanovehicles are often made from macromolecular materials such as poly(lactide-*co*-glycolide) (PLGA), chitosan and poly-hydroxyethyl methacrylate/stearic acid, forming dendrimer, liposomes,[7,8] polymers[9] and inorganic nanoparticles.[10] Among them, chitosan (CS) is a cationic natural polysaccharide obtained by deacetylation of chitin, being the second most abundant biopolymer on the earth after cellulose.[11,12] CS is also known to be a promising biomaterial due to its biodegradability, non-toxicity, biocompatibility and immunogenicity.[13–15] However, the poor water-solubility of CS limits its application in drug delivery.[16] In our previous study, the low molecular weight amphiphilic oligo-chitosan, which was able to self-assemble into nanomicelles in water, was synthesized

[a]*Department of Pharmacology, School of Basic Medical Sciences, Capital Medical University, Beijing, P.R. China. E-mail: yumingzhao@ccmu.edu.cn*
[b]*State Key Laboratory for Structural Chemistry of Unstable and Stable Species, Institute of Chemistry, Chinese Academy of Sciences, 100190, Beijing, P. R. China*
[c]*School of Biomedical Engineering, Capital Medical University, Beijing, China*
[d]*School of Pharmaceutical Sciences, Capital Medical University, Beijing, P. R. China*
[e]*Institute of Chinese Medical Sciences, State Key Laboratory of Quality Research in Chinese Medicine, University of Macau, Macao, P. R. China*
† These authors contribute equally to the work.

through conjugating multiple hydroxylethyl groups.[17,18] The prepared ultra-small and amphiphilic CS could deliver the antioxidant (trolox) into the treated cells promptly with high antioxidative performance and low side effects. It implied that the amphiphilic CS nanoparticles might be an optimal drug delivery system in anti-cancer nanomedicine.

Another challenge facing chemotherapy today is how to simultaneously delivery therapeutics agent and image or track the responses of cancer cells *in vivo* or *in vitro*, *i.e.* tumour theranostics.[19,20] To observe the actions of the cancer cells, the fluorescent probes, such as organic dye[20] and quantum dots (QDs)[21,22] have been extensively investigated in cell imaging. However, the poor photostability of organic dye and the toxicity of QDs limit their application in clinic.[23] Gold nanoclusters (Au NCs) of ~2 nm in size are attractive in tumour imaging due to the strong luminescence, stable photostability, low toxicity and surface functionalities.[24,25] It has been proved that the hydrodynamic size (<3 nm) is relatively small which could be effectively eliminated through renal.[26,27]

Based on the aforementioned considerations, a chitosan-based nanovehicles which are capable of cancer cells imaging and targeted drug delivery were synthesized. A schematic diagram of synthesis route for the methotrexate (MTX)-encapsulated chitosan nanocomposites (*i.e.* MTX@AuNCs-CS–AS1411) has been exhibited in the Fig. 1. The AuNCs conjugated CS nanovehicles (AuNCs-CS) was synthesized by covalent reaction and then conjugated with anti-nucleolin aptamer (AS1411) for site-specific targeting against tumour cells that overexpress nucleolin receptors.[28,29] A hydrophobic model anticancer drug, methotrexate (MTX) was finally encapsulated into the tumour-targeted nanovehicles through hydrophobic interaction. In our recent study, it was proved that the MTX@AuNCs-CS–AS1411 could be specifically targeted to the lung cancer cells *in vivo* and *in vitro*.[29] However, whether the AuNCs-CS–AS1411 nanovehicles could illustrate the extensive "all in one" properties in hepatocellular carcinoma are still unknown. Herein, the structure and properties of prepared the tumour-targeted nanovehicles were characterized and determined by fluorescence, UV-visible absorption, transmission electron microscope (TEM), dynamic light scattering (DLS), Fourier transform infrared (FT-IR) and X-ray photoelectron spectroscopy (XPS). Compared with the behaviours in human normal hepatic cell line LO2, the selectivity and targeting properties of MTX@AuNCs-CS–AS1411 were demonstrated for human hepatocellular carcinoma cell line HepG2. The *in vitro* cytotoxicity and cellular uptake of AuNCs-CS–AS1411 was also comparatively evaluated in HepG2 and LO2.

Material and methods

Materials

CS (MW = 80 kDa, degree of deacetylation = 85%), glutathione, methotrexate, 3-(4,5-dimethylthiazol-2-yl)-2,5-diphenyl tetrazolium bromide (MTT), Hoechst 33342, 1-ethyl-3-(3-dimethylaminopropyl) carbodiimide hydrochloride (EDC), rhodamine B and hydrogen tetrachloroaureate(III) trihydrate ($HAuCl_4 \cdot 3H_2O$) were purchased from Sigma-Aldrich (St Louis, MO, USA). Annexin V-FITC/propidine iodide (PI) double staining kit was purchased from Solarbio Biotech (Beijing, China). Dulbecco's modified Eagle's medium (DMEM), fetal bovine serum, penicillin, streptomycin and phosphate buffered saline (PBS) were purchased from Thermo Fisher Co. (Beijing, China). Aptamer AS1411 (5′-GGTGGTGGTGGTTGTGGTG GTGGT GG-3′) were purchased from Sangon Biotech Co. (Shanghai, China). Unless specified, all other reagents were of analytical grade.

Instruments

FT-IR spectra were collected on a Bruker Tensor-27 Fourier transform infrared spectrometer (Bruker, Germany). UV-visible absorption spectra were detected by a Hitachi UV-3310

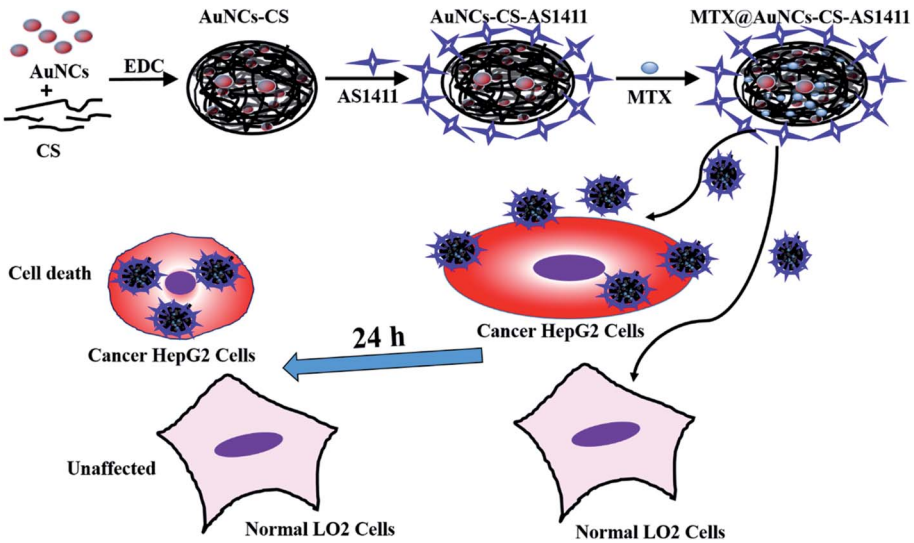

Fig. 1 Schematic illustration of the synthesis of the MTX@AuNCs-CS–AS1411, and its targeted delivery and imaging of cancer cells. In brief, facilitated by the fluorescence from Au clusters, the MTX@AuNCs-CS–AS1411 could be bio-tracked. Study showed that MTX@AuNCs-CS–AS1411 could specifically target to the cancer HepG2 cells and cause cell death possibly through apoptosis.

spectrophotometer (Tokyo, Japan). Fluorescence intensities were measured by a Hitachi F-2500 fluorescence spectrometer (Tokyo, Japan). X-ray photoelectron spectroscopy (XPS) measurements were recorded on an ESCALab220i-XL (VG, England). Zeta potential was conducted on a Zetasizer nano ZS (ZEN3600) instrument (Malvern, England). The absorbance for MTT reduction assay was recorded with a microplate reader (BIO-TEK Synergy HT, USA) at 570 nm. Cell imaging was recorded by Olympus IX81 confocal laser scanning microscope. All measurements were performed at room temperature.

Synthesis of AuNCs

AuNCs was prepared as previously described.[30] Briefly, $HAuCl_4 \cdot 3H_2O$ (2.5 mM, 5 mL) and the reduced glutathione (GSH) (2.5 mM, 5 mL) was stirred at 32 °C under room light. After 36 h, 5 mL of GSH (2.5 mM) was added, and the reaction was continued for another 6 h. The solution was first centrifuged at 13 000 rpm for 30 min, and then the supernatant was further dialyzed for 2 d to remove the non-reactive species. The final product (*i.e.* AuNCs) was freeze-dried overnight.

Synthesis of fluorescent nanovehicles: AuNCs-CS

AuNCs in PBS (pH 6.0, 5 mL) was activated with EDC (0.02 g) at 0 °C for 2 h. Then, CS (0.1 g) was added and the mixture was stirred for 24 h. The resulting solution was further dialyzed for 3 d and then freeze-dried.

Synthesis of dual-functional nanovehicles: AuNCs-CS–AS1411

Firstly, 0.05 g AuNCs-CS was dissolved in 5 mL water and AS1411 aptamer (10 μL, 100 μM) was added. The reaction was allowed for 1 h at the room temperature. The product was centrifuged at 15000 rpm for 10 min to remove non-reactive AS1411. Supernatant was dissolved in 5 mL water. The product was stored at −20 °C.

Drug loading and release

To evaluate the drug loading and release properties of the dual-functional nanovehicle, the MTX was chosen as a model anti-cancer drug. 0.01 g MTX was added into AuNCs-CS–ASL1411 (2 mL), and shaken 2 h. Then, the mixture was centrifuged at 4000 rpm to remove the excess MTX. The supernatant was further filtered by 0.45 μm pellicle and dissolved in water.

The drug release rate was measured by dispersing the nanodrug (MTX@AuNCs–AS1411) in PBS buffer with different pH values (pH 5.5, 7.4) and the solution was stirring at room temperature. The concentration of released MTX was determined by UV-vis spectroscopy at $\lambda_{max} = 306$ nm.

Cell culture

The human hepatocellular carcinoma cell line HepG2 and normal liver cell line LO2 were from the American Type Culture Collection (ATCC). All the cells were cultured in DMEM medium supplemented with 10% FBS. Culture was maintained in a humidified incubator (5% CO_2) at 37 °C.

Cellular uptake and targeted imaging of AuNCs-CS–AS1411

HepG2 cells and LO2 cells were seeded with a density of 1.5×10^4 cells per cm^2 in confocal plates, respectively. The cells were washed with PBS (pH 7.4) and suspended in 1 mL of 200 μg mL^{-1} AuNCs-CS–AS1411. Cellular uptake of AuNCs-CS–AS1411 were observed after incubation of the nanomedicine for different time (1 h, 2 h and 4 h), the cells were washed with PBS and subjected to fluorescence microscopy examination. The fluorescence images were acquired by the confocal microscope at the excitation of wavelength 559 nm.

Cytotoxicity and apoptosis assays

The cell viability was determined by MTT reduction assay to evaluate the cytotoxicity of nanocomposite. In brief, the HepG2 cells and LO2 cells were seeded at a density of 0.5×10^4 cells in 96-well plates, and then incubated with AuNCs-CS, AuNCs-CS–AS1411, MTX, MTX@AuNCs-CS and MTX@ AuNCs-CS–AS1411 in different concentration. The culture was maintained at standard culture condition under 37 °C for 24 h. Then each well was replaced and washed with PBS (pH 7.4) and 0.1 mL MTT solution (0.5 mg mL^{-1} in DMEM) was added into each well. After incubation for another 4 h, the medium was carefully removed from each well and 150 μL of dimethyl sulfoxide was added. After shaking the plates for 10 min, the absorbance values (OD) was measured at 570 nm with a microplate reader. The cell viability was estimated by the following equation: viable cells (%) = $(OD_{treated}/OD_{control}) \times 100\%$, where $OD_{treated}$ was obtained in the presence of AuNCs-CS, AuNCs-CS–AS1411, MTX, MTX@AuNCs-CS and MTX@ AuNCs-CS–AS1411; $OD_{control}$ represents the absorbance of the control group recorded in the incubation medium.

Hoechst 33342 staining was used to detect the chromatin condensation. Briefly, the HepG2 cells and LO2 cells were incubated with MTX (20 μg mL^{-1}), MTX@AuNCs-CS and MTX@AuNCs-CS–AS1411 for 24 h, then Hoechst 33342 (5 μg mL^{-1}) was added and incubated for 10 min. The images were collected using a fluorescence microscope at 400 fold of magnification. The apoptotic cells showed condensed or fragmented fluorescent nuclei. Numbers of apoptotic nuclei were scored by counting at least 500 cells for each group in triplicate.

The apoptosis status of HepG2 cells and LO2 cells was analyzed using Annexin V-FITC/PI double staining according to the manual instruction (Solarbio, Beijing, China). Briefly, after treatment, the cells were harvested and washed with PBS buffer for 2 times. Then the binding buffer was added to the resuspended cells and 5 μL Annexin V-FITC reagent was added and incubated in dark for 15 min. Then 5 μL PI was added before detection. Afterwards, the sample was analyzed by flow cytometry (C6, BD). In this study, Annexin V positive cells were considered as apoptotic cells.

Statistical analysis

Data were presented as the Mean ± Standard Deviation (SD). Statistical analyses were performed using SPSS version 18.0 software (SPSS Inc., Chicago, IL). Student's *t*-test for unpaired data was used to evaluate statistical differences. Statistically significant were considered at $P < 0.05$.

Results

The preparation and characterization of AuNCs-CS–AS1411

As shown in the Fig. 1, AuNCs was synthesized according to the previous literature,[31] and then AuNCs was conjugated onto the CS by covalent binding reaction. Next, the AuNCs-CS was functionalized with the anti-nucleolin aptamer AS1411 to produce the dual-functional nanovehicles: AuNCs-CS–AS1411. Then, a hydrophobic model anticancer drug, methotrexate (MTX) was successfully loaded into the nanovehicles through hydrophobic interaction.

The structures of AuNCs-CS–AS1411, AuNCs-CS as well as AuNCs were comparatively characterized by FT-IR (Fig. 2A), UV and fluorescence (Fig. 2B) and XPS (Fig. 2C and D). Compared with FT-IR spectrum of the AuNCs, the FT-IR peak of AuNCs-CS at 1730 cm^{-1} which represented the stretching vibration of C=O bond from carboxyl groups was disappeared, while the peak intensity at 1644 cm^{-1} (stretching vibration of C=O bond from amide) was obviously enhanced. The evidences reasonably demonstrated that new amide bonds were formed between the carboxyl groups in AuNCs and amine groups from CS, and therefore the AuNCs-CS was covalently conjugated. The results of UV-visible spectroscopy and fluorescence spectroscopy, as shown in Fig. 2B, further indicated that there were no characteristic broad surface plasmon resonance (SPR) band peaked around 520 nm for AuNCs and AuNCs-CS–AS1411, thus suggesting that the core diameters of the two types of gold clusters were less than 2 nm.[32] The emission of AuNCs peaked at 607 nm when excited at 396 nm. Its fluorescent intensity was slightly reduced once the AuNCs was conjugated onto the CS, and being accompanied by a slight red-shift to 609 nm. Both AuNCs and AuNCs-CS–AS1411 could be dispersed in water, forming a faint yellow solution. Under UV irradiation at 365 nm, the aqueous dispersions emitted red luminescence. XPS survey spectra (Fig. 2D) showed that both AuNCs and AuNCs-CS contained C, N, O, S and Au elements, and there existed a little residual chlorine in AuNCs, which may origin from $HAuCl_4$. For AuNCs-CS, the relative content of carbon (C1s peak) was increased by 10.3% and the relative contents of sulfur (S2p peak) and nitrogen (N1s peak) were decreased by 2.01% and 4.97% after being conjugated with the CS, respectively. XPS measurements (Fig. 2C) also showed that the binding energies of Au 4f7/2 of AuNCs and AuNCs-CS were located at 84.22 eV and 84.27 eV, respectively. These values are near to the binding energy of 4f7/2 of zero-valent Au (84.0 eV) and therefore suggest that there is no strong chemical binding between AuNCs and nearby ligands.

The particle size, distribution, and morphology of the nanoparticles were examined by means of TEM (Fig. 3A and B) and DLS (Fig. 3C), respectively. TEM images showed that the gold nanoclusters (AuNCs) in the study were basically spherical ball in shape and well-dispersed with a diameter ranged from 1.5 nm up to 2.1 nm (Fig. 3A). AuNCs-CS–AS1411 also appeared nearly spherical ball in shape, but the size of particles ranged from 24 nm to 36 nm in diameter (Fig. 3B). The inset in Fig. 3B further exhibited that there are small dark particles distributed inside the chitosan balls, indicating that the fluorescent AuNCs were successfully conjugated into the CS. Furthermore, statistical analysis of DLS data in Fig. 3C showed that the hydrodynamic size of CS, AuNCs-CS, AuNCs-CS–AS1411 and MTX@AuNCs-CS–AS1411 are 183 ± 3.5 nm, 192 ± 6.5 nm, 200 ± 4 nm and 210 ± 9.5 nm, respectively (Fig. 3D).

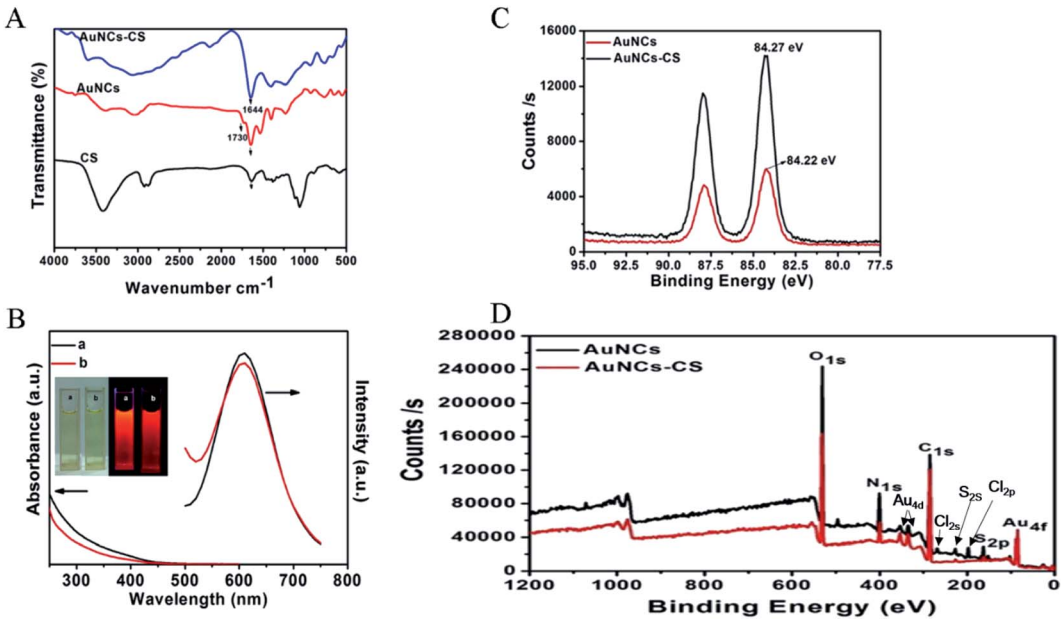

Fig. 2 Characterizations of AuNCs-CS. (A) FT-IR spectrum of CS, AuNCs and AuNCs-CS. (B) UV-Vis absorption spectra and fluorescence emission spectra of (a) AuNCs and (b) AuNCs-CS–AS1411. Insets in (B) showed the photos of the dispersions of the AuNCs (a) and the AuNCs-CS (b) under daylight (left) and UV light at 365 nm (right). XPS full spectra of AuNCs and AuNCs-CS. (C) XPS survey of Au(4f7/2) obtained from AuNCs and AuNCs-CS (D).

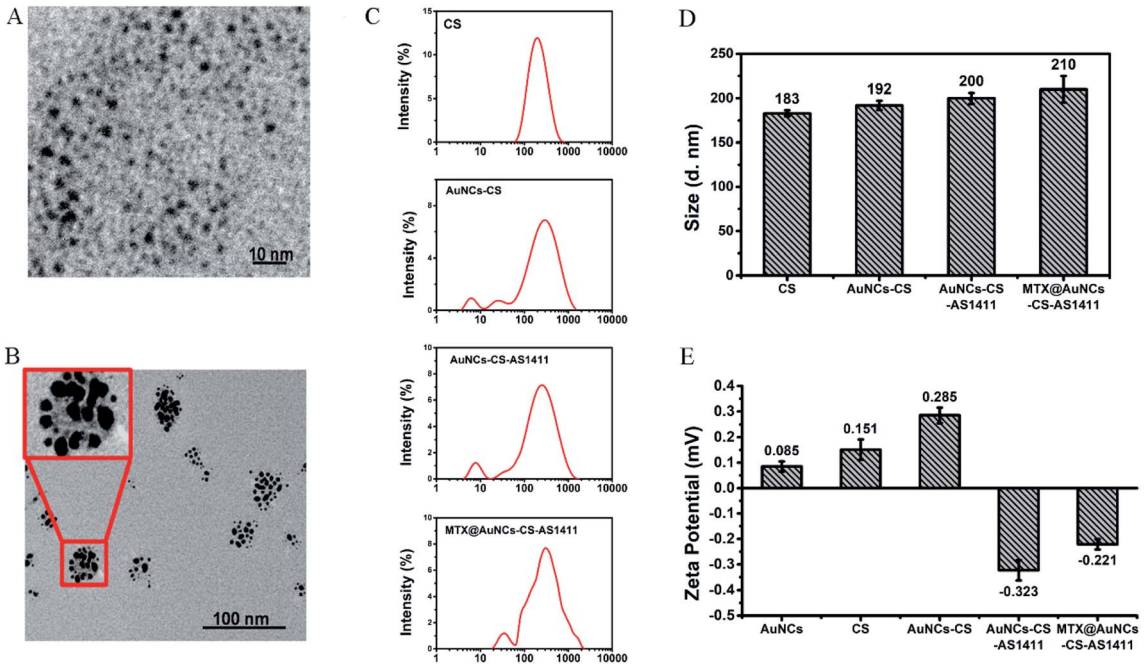

Fig. 3 The TEM of the AuNCs (A) and AuNCs-CS–AS1411 (B). The inset in (B) is the enlarge image of AuNCs-CS–AS1411 in rectangle region. DLS curves of CS, AuNCs-CS, AuNCs-CS–AS1411 and MTX@AuNCs-CS–AS1411 (C). The statistics of the hydrodynamic size of the related nanoparticles (D). Zeta potentials of the nanoparticles (E).

It is also confirmed that the zeta potentials of AuNCs, CS, AuNCs-CS, AuNCs-CS–AS1411 and MTX@AuNCs-CS–AS1411 were 0.085 ± 0.009 mV, 0.15 ± 0.01 mV, 0.285 ± 0.018 mV, −0.323 ± 0.024 mV and −0.221 ± 0.008 (Fig. 3E), respectively. The reason why the zeta-potential of AuNCs-CS–AS1411 were shifted to more negative direction (about −0.323 mV) is probably caused by the electrostatic interaction between the positive charged chitosan (core) and the negatively charged DNA aptamers (shell) on the surface of dual-functional nanovehicles.

Stability of AuNCs-CS–AS1411

After 600 s of UV-irradiation, the AuNCs-CS–AS1411 kept 95% of its original fluorescence while the rhodamine B dye retained only 76% of its original value (Fig. 4A). Furthermore, there were no apparent changes in fluorescent profiles under different pH values (pH 5.5, 7.4 and 8.5), respectively which implied that the nanovehicles remained stable under neutral, weak acidic and weak alkaline conditions (Fig. 4B). And Fig. 4C exhibited that the fluorescent nanocomposites of AuNCs-CS–AS1411 could still keep stable in PBS (10 mM, pH 7.4) even after one month of incubation.

Drug loading and release

The UV-visible spectroscopy survey revealed that both MTX monomer and MTX@AuNCs-CS–AS1411 showed strong absorption at 303 nm (Fig. 5A), and meanwhile the drug-loading efficiency of MTX by the dual-functional nanovehicles (AuNCs-CS–AS1411) was calculated as 14.2%. The *in vitro* MTX release behaviours from MTX@AuNCs-CS–AS1411 were evaluated in PBS buffers with different pH values (pH 5.5 and pH 7.4) at room temperature, respectively (Fig. 5B). After 2.5 h of incubation, 62% of MTX was promptly released from the nanovehicles at pH 5.5, but only 28% of drug was released at pH 7.4. And after 24 h of incubation, the cumulative release percentage of MTX was 93% at pH 5.5, while roughly total of 72% of drug was released at pH 7.4. Interestingly, the MTX release from the MTX@AuNCs-CS–AS1411 was much faster in the mildly acidic solution (*i.e.* mimicking endosome/lysosome conditions) than in near-neutral environment (*i.e.* mimicking blood or other body fluids). The pH-sensitive drug release may provide a possibility of more efficiently release of MTX in the acidic microenvironment as in intracellular lysosome of tumour cells.

The cellular uptake and targeted imaging of hepatic cancer cells

It has been reported that nucleolin is highly overexpressed on the surface of tumour cells, such as hepatic cancer cells, but not on the surface of normal pulmonary or hepatic cells. As a result, to explore and examine the targeting effect of the AS1411-guided nanovehicles on hepatic cancer cells, the cellular uptakes of AuNCs-CS–AS1411 into HepG2 and LO2 were comparatively performed by using confocal laser scanning microscopy. As shown in the top row of Fig. 6A, only a weak fluorescent signal was observed inside HepG2 under 1 h of incubation. Afterwards, with an increase of incubation time, the fluorescent signals became gradually intense, implying that the more and more fluorescent nanovehicles were taken up by hepatic cancer cells. In contrast to HepG2, the LO2 cells displayed very faint fluorescence even after 4 h of incubation (down row of Fig. 6A). The partial enlarged cell imaging on the right

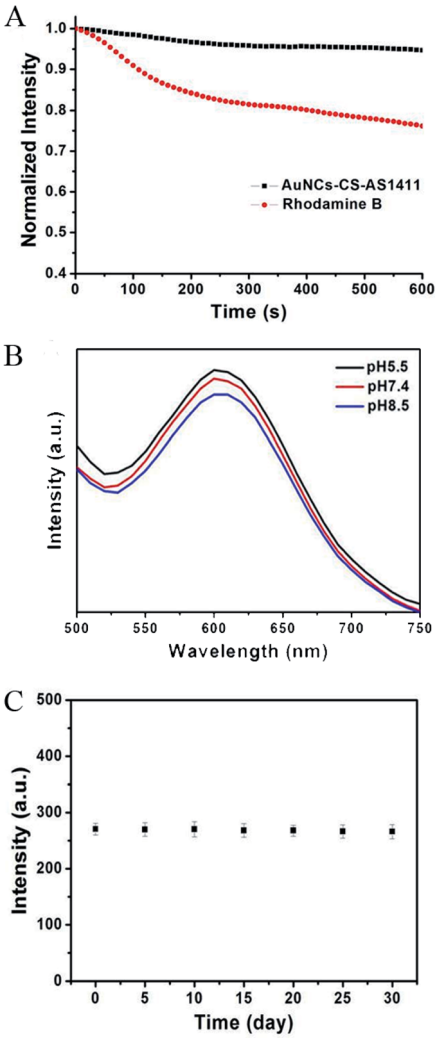

Fig. 4 Photostability detection of AuNCs-CS–AS1411. (A) Photostability of AuNCs-CS–AS1411 and rhodamine B in PBS (pH 7.4) with a 150 W xenon lamp excitation source. Fluorescence intensity of AuNCs-CS–AS1411 (200 μg mL^{-1}) in PBS (10 mM) solution at different pH (B) and stored in PBS (10 mM, pH 7.4) for different periods (C).

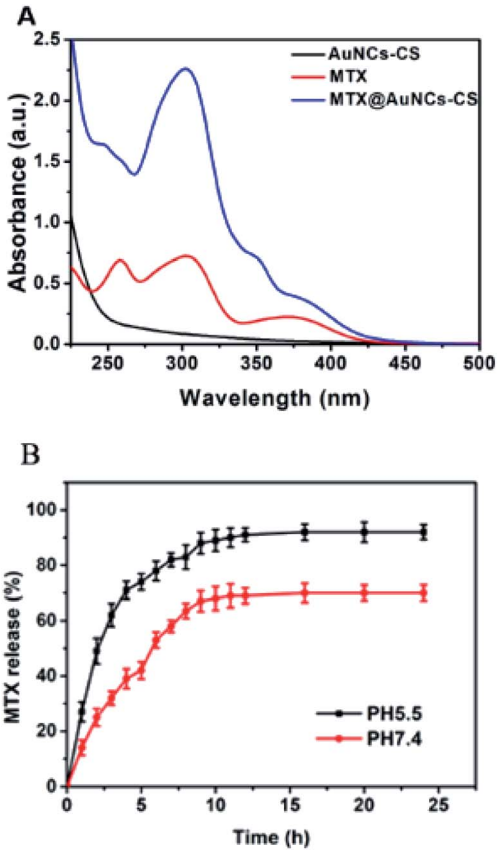

Fig. 5 *In vitro* MTX loading and release behaviours evaluated by UV–visible absorption spectra (A) UV-visible absorption spectra of AuNCs-CS, MTX and MTX@AuNCs-CS–AS1411; (B) the release behaviors of MTX from MTX@AuNCs-CS–AS1411 in PBS (10 mM) at pH 5.5 and pH 7.4, respectively.

side of Fig. 6A more clearly presented the difference of fluorescent intensities between these two cell types. Statistical analysis of average fluorescence intensity in the two cell populations with different incubation times (1 h, 2 h and 4 h) quantitatively revealed the significant difference between HepG2 and LO2 (Fig. 6B) and further indicated that the MTX uptake by HepG2 was roughly 3.7 folds of that by LO2.

In vitro cytotoxicity and apoptosis induction

In order to evaluate the *in vitro* targeted chemotherapy efficiency of MTX@AuNCs-CS–AS1411, the cytotoxicity and apoptosis induction of MTX-encapsulating chitosan-based nanovehicles and empty nano-vehicles against hepatic cancer cells and normal hepatic cells were comparatively examined using MTT assay, Hoechst staining and flow cytometry assay. The cell survival studies were initially performed with empty dual-functional nanovehicles (AuNCs-CS–AS1411) on HepG2 and LO2 cells to test whether the chitosan-based nanovehicles themselves contributed to the cytotoxicity. As shown in Fig. 7A, no significant cytotoxicity was observed in HepG2 and LO2 cells after 24 h incubation with the empty nanovehicles, even at the concentrations as high as 200 μg mL^{-1}. The viability of the surviving cells treated with MTX, the empty nanovehicles and the nanovehicles encapsulating MTX were further presented in Fig. 7B. Compared to MTX@AuNCs-CS, the dual-functional nano-drug (*i.e.* MTX@AuNCs-CS–AS1411) yielded a significantly reduction of the cell viability (58% to 38%) and exerted more toxic effects on HepG2. The toxicity of MTX@AuNCs-CS–AS1411 to HepG2 was significantly more intensive than that to LO2. However, MTX@AuNCs-CS–AS1411 did not cause more toxic effects than MTX@AuNCs-CS did on LO2 cells since both nanovehicles encapsulating MTXs (*i.e.* MTX@AuNCs-CS–AS1411 and MTX@AuNCs-CS) exhibited nearly identical cell viability for normal hepatic cells, 58% and 59%, respectively.

To comparatively examine apoptosis-inducing effect, confocal images of HepG2 and LO2 cells stained with Hoechst 33342 were obtained upon the addition of MTX@AuNCs-CS–AS1411, MTX@AuNCs-CS, MTX and normal saline. As illustrated in the left picture of Fig. 7C, the white arrows indicated

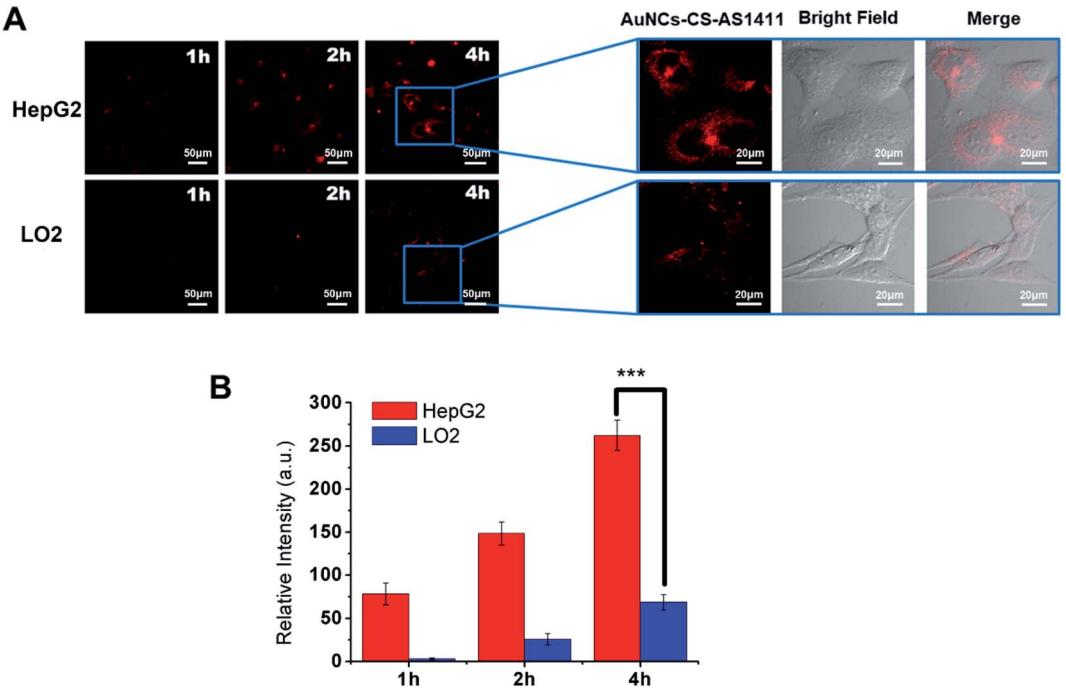

Fig. 6 The cellular uptake and imaging of AuNCs-CS–AS1411 in HepG2 cells and LO2 cells. (A) Intracellular trafficking of AuNCs-CS–AS1411 (20 μg mL^{-1}) after incubation with HepG2 cells and LO2 cells for 1 h, 2 h and 4 h; images in rectangular regions were magnified in the upper right lanes. (B) Statistical analysis of the fluorescence intensity of HepG2 cells and LO2 cells after treated with AuNCs-CS–AS1411 for different time (1 h, 2 h and 4 h). Excitation wavelength: 559 nm. Values are Mean ± Standard Deviation (SD). ***$P < 0.001$*vs.* HepG2 cells.

the condensed DNA and fragmented nuclei which occurred in the apoptotic cells. The quantification of the percentage of apoptotic cells was estimated based on statistical analysis of the nuclei morphology (see the right graph of Fig. 7C). The apoptosis-induction ability of MTX@AuNCs-CS–AS1411 was further analyzed by flow cytometry assay using the Annexin V-FITC/PI double staining. In each panel of Fig. 7D (see left image), the lower-left (Annexin V-FITC−, PI−), lower-right (Annexin V-FITC+, PI−) and upper-right (Annexin V-FITC+, PI+) quadrants represent the populations of live cells, early apoptotic cells and late apoptotic cells, respectively. The average percentage of apoptotic cells, including early apoptotic cells and late apoptotic cells, in each case was further exhibited in right graph of Fig. 7D. Similar apoptosis-inducing trends were observed in Hoechst 33342 staining and flow cytometry assay by Annexin IV/PI labelling. Both analyses for apoptosis inducing activity indicated that only the dual-functional nano-drug MTX@AuNCs-CS–AS1411 exhibited stronger apoptosis-inducing potency in hepatic cancer cells, rather than in normal hepatic cells. Therefore, the MTX@AuNCs-CS–AS1411 are considered as potential tumour-therapeutic nano-drug because such a nucleolin-specific MTX transport and releasing could induce the death of hepatic cancer cells, probably *via* apoptosis, leaving the normal hepatic cells not injured or less harmed.

Discussion

Hepatocellular carcinoma (HCC) accounts for 75–85% of primary liver cancers, which is predicted to be the fourth leading cause of cancer deaths worldwide in 2018.[33,34] In China, around 383 000 people die from liver cancer each year. In the early stages, surgical interventions are suitable curative treatments.[35,36] However, the surgical treatments do not work effectively in the advanced stages. Chemotherapy is the most effective treatment in HCC therapy but strictly limited because of the poor targeting efficiency and serious side effects.[37] Under this situation, nanometer-sized controlled drug delivery systems based on macromolecular materials provide indubitable benefits for chemotherapy patients in improving targeting efficiency and reducing side effects.

Chitosan is obtained from the deacetylation of chitin. It is composed of β-(1,4)-linked glucosamine units (2-amino-2-deoxy-β-D-glucopyranose) and *N*-acetylglucosamine units (2-acetamino-2-deoxy-β-D-glucopyranose) in different ratios.[38] The amino group on chitosan provided controlled release, permeation enhancement, mucoadhesion, *in situ* gelation.[39] The chitosan-based delivery system has been investigated in hepatocellular carcinoma treatment which illustrated desirable anti-hepatocellular carcinoma effects.[33,40] For instance, delivered by the CS nanovehicle system, liver-specific miRNA-122 and anti-cancer drug 5-fluorouracil (5-Fu) using a macromolecular pro-drug approach significantly decrease the hepatocellular carcinoma tumour size *in vivo*.[33]

In addition, chitosan with silica co-encapsulated curcumin nanoparticles showed potential anti-hepatocellular carcinoma effects *in vivo* and *in vitro*.[40] In our previous study, a serial of small size nanocarriers by degraded low molecular weight chitosan were synthesized to improve the drug solubility and the bioavailability. Facilitated by the chitosan nanovehicles,

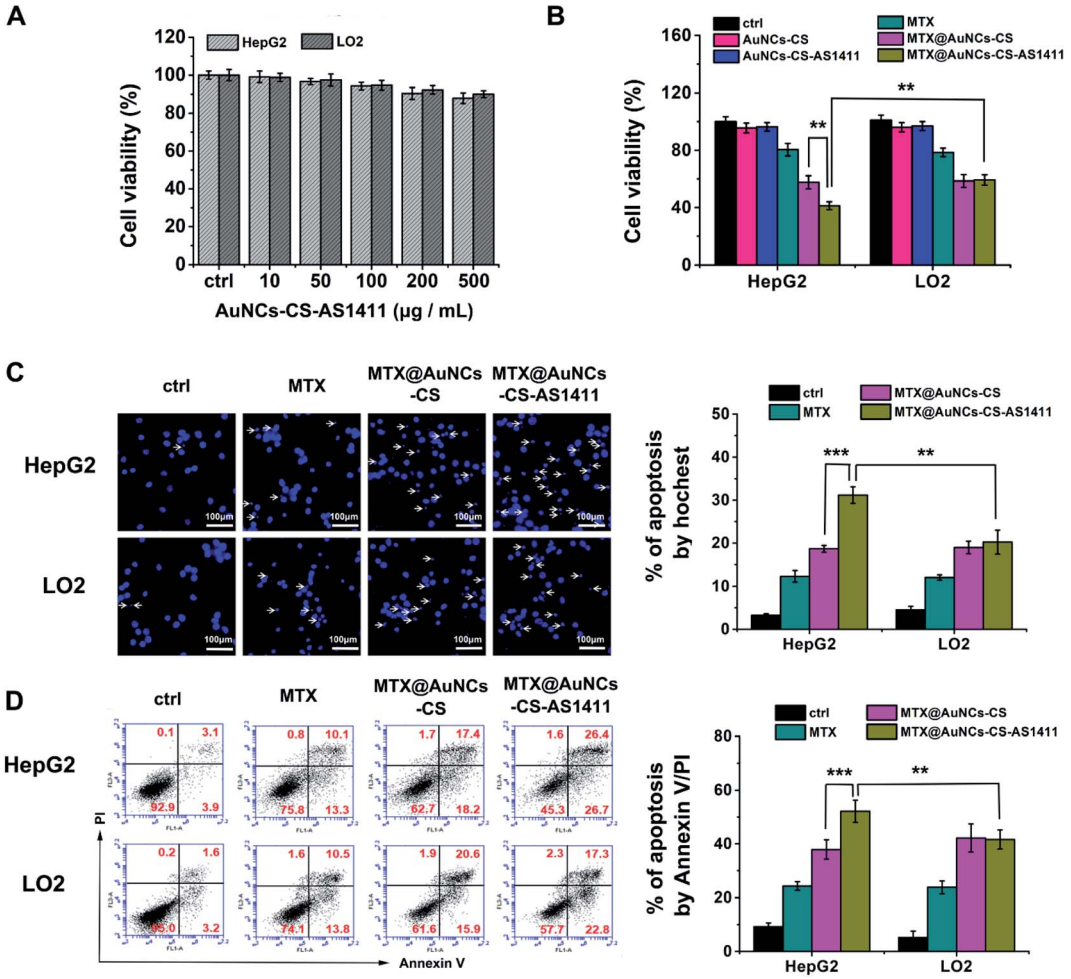

Fig. 7 The anti-cancer effects of MTX@AuNCs-CS–AS1411 in HepG2 cells and LO2 cells. (A, B) Cell viability was detected by MTT reduction assay. (A)The *in vitro* cytotoxicity of AuNCs-CS–AS1411 in HepG2 cells and LO2 cells after incubation with different concentration for 24 h; (B) the cell viability of HepG2 cells and LO2 cells after incubation with AuNCs-CS, AuNCs-CS–AS1411, MTX, MTX@AuNCs-CS and MTX@AuNCs-CS–AS1411 for 24 h. (C)The chromatin condensation was detected using Hoechst 33342 staining in HepG2 cells and LO2 cells after incubation with MTX, MTX@AuNCs-CS and MTX@AuNCs-CS–AS1411 for 24 h. The representative images were shown on the left and the statistical results were shown on the right. (D) The apoptosis was analyzed using Annexin V-FITC/PI double staining in HepG2 cells and LO2 cells after incubation with MTX, MTX@AuNCs-CS and MTX@AuNCs-CS–AS1411 for 24 h. The representative images were shown on the left and the statistical results were shown on the right. Values are Mean ± Standard Deviation (SD). $^{**}P < 0.01$, $^{***}P < 0.001$ *vs.* AuNCs-CS–AS1411 treated HepG2 cells.

antioxidant of trolox showed enhanced anti-oxidative effects on macrophage RAW264.7 cells and PC 12 cells.[17,18] Based on these investigations, chitosan encapsulating nano drugs were first synthesized and showed significant chemotherapy effects on lung cancer *in vivo* and *in vitro*.[29]

The controlled release experiments show that the release of MTX from MTX@AuNCs-CS–AS1411 is pH-dependent which is likely due to that chitosan (CS) is a natural cationic pH-responsive polymer and exhibits pH-sensitive swelling. Due to protonation of amino groups in CS at lower pH, strong electrostatic repulsion occurs between the CS chains and initiates drug-releasing under acidic conditions. On the other hand, the intermolecular hydrogen-bonding interaction between CS chains and MTX is also pH-responsive.[41] The pK_{a1} and pK_{a2} values of two amino groups in MTX are 4.84 and 5.51, respectively, so that amino groups of MTX can be partially protonated and transform into its protonation form ($-NH_3^+$) at pH 5.5, by which the intermolecular hydrogen bonding become weak and finally results in an acidic-responsive release properties of the nanovehicle.

Nucleic acid aptamers are synthetic, short, single-stranded DNA or RNA molecules which are able to recognize and high specifically bind to some molecules, cells and even whole organisms.[42] They are considered as promising ligands for active targeting in oncology. AS1411 aptamer, also known as AGRO100, is among the aptamers most extensively studied and used. And it is a 26-mer unmodified guanosine (G)-rich oligonucleotide [5′-d(GGT GGT GGT GGT TGT GGT GGT GGT GG)-3′] that binds specifically to nucleolin, a protein located on the surface and in the cytoplasm of most malignant tumour cells but absent from the surface/cytoplasm of most normal cells. As a result, AS1411 has shown promising clinical activities and is

being widely used as a tumour-targeting agent for breast cancer,[43] gastric cancer,[44] malignant melanomas[45] and glioblastoma.[46] Despite its many advances in drug delivery for cancer treatment, the delivery efficacy of AS1411 against some malignant tumours, such as non-small cell lung cancer (NSCLC) and HCC, still remains ambiguous. Therefore, our team developed a dual-functional nanovehicle through electrostatic interaction between the fluorescent gold nanocluster-conjugated chitosan and AS1411 aptamer. Herein, the nanovehicle was further verified whether it can be used for the treatment of hepatocellular carcinoma tumors and concurrently bio-imaging the tumour cells while having low toxicity toward normal cells.

As reported in our prior work,[29] free drug (MTX), the fluorescent nanovehicle encapsulating MTX (MTX@AuNCs-CS) and dual-functional nanovehicle encapsulating MTX (MTX@AuNCs-CS–AS1411) exhibited *in vitro* toxicity to human non-small cell lung cancer cell line (A549 cells) at the concentration of 100 μg mL^{-1} with the corresponding apoptosis rate of 31%, 36% and 42%, respectively. In the current study, although free drug (MTX) only show cytotoxicity to human hepatocellular carcinoma cell line (HepG2) at the concentration of 20 μg mL^{-1} with the corresponding apoptosis rate of 23%, MTX@AuNCs-CS and MTX@AuNCs-CS–AS1411 exhibits cytotoxicity in the same condition with the corresponding apoptosis rate of 38% and 51%, respectively (See Fig. 7D). Apparently, the rates of cell proliferation inhibition and apoptosis in HepG2 cells treated with the nanovehicle encapsulating MTX, including MTX@AuNCs-CS and MTX@AuNCs-CS–AS1411, were significantly higher than those in A549 cells, even using much lower chemotherapeutic doses of MTX (20 μg mL^{-1}). It might imply that the nanovehicle encapsulating MTX probably could be more sensitive to HepG2 and could achieve better therapeutic effects in patients with HCC.

The aim of nanotheranostics is to bundle the therapeutic and diagnostic capabilities into one unit *via* a single nanovehicle, thereby simultaneously delivering therapeutics agent and real-time monitoring the treatment response. More recently, Li *et al.* reported a new carbon quantum dots (CQDs) that can bind to the large neutral amino acid transporter 1 (LAT-1) which is overexpressed in the majority of carcinoma cells but not in normal tissues.[47] The versatility of functionalization and high tumour selectivity of the CQDs make them broadly suitable for tumour-specific imaging and drug delivery. Referring to this report, our studies imply that the new AuNCs-CS–AS1411 nanovehicle might become another potential candidate of theranostic nanoplatform for treating and monitoring a broad range of malignant tumour tissues.

Conclusions

Based on the fluorescent AuNCs, a dual-functional nanovehicle (AuNCs-CS–AS1411) was successfully synthesized and used for targeted drug delivery and fluorescent imaging of tumour cells. The nanovehicle also shows many advantages such as good photostability, low cytotoxicity and controlled drug release. With the aid of aptamer AS1411, the nanocarrier exhibits high-specific tumour cells targeting and results in the enhancing cytotoxicity and apoptosis-inducing activity against human hepatocellular carcinoma cells. In contrast, it only shows weak cytotoxicity against human normal liver cells. In combination with our previous work, the present results further suggest that the AuNCs-CS–AS1411 nanovehicle may provide a new theranostic strategy for simultaneously treating and monitoring a broad range of malignant tumors, including HCC and NSCLC. As a result, we are planning to verify the tumour-specific apoptosis-inducing activity against liver cancer *in vivo*, and to evaluate the real potential of MTX@AuNCs-CS–AS1411 in clinical applications.

Author contributions

Dr Xiaojie Zhang, Mr Qiming Gao, Dr Qianfen Zhuang and Dr Lu Zhang contribute equally to the work, who are performed the majority of the investigations. Miss Sihan Wang, Ms. Qiu Tian, Dr Libo Du, Miss Wenxi Yuan, Dr Caifang Wang and Dr Hua Yu are responsible for the data curation and formal analysis. Dr Yuming Zhao and Dr Yang Liu are responsible for conceptualization, supervision and validation the research.

Conflicts of interest

There are no conflicts to declare.

Acknowledgements

The authors gratefully acknowledge the financial support from the National Natural Science Foundation of China (31570856, 31741035, 32000880), the project of Beijing (China) Education Commission (KM201610025007). The authors sincerely thank Mr Seewald Jamie Lachlan for proofing our manuscript.

References

1 F. Bray, J. Ferlay, I. Soerjomataram, R. L. Siegel, L. A. Torre and A. Jemal, *Ca-Cancer J. Clin.*, 2018, **68**, 394–424.
2 W. Chen, R. Zheng, P. D. Baade, S. Zhang, H. Zeng, F. Bray, A. Jemal, X. Q. Yu and J. He, *Ca-Cancer J. Clin.*, 2016, **66**, 115–132.
3 B. Jing, G. Cheng, J. Li, Z. A. Wang and Y. Du, *Mar. Drugs*, 2019, **17**, 415.
4 D. H. Henry, C. J. Langer, R. S. McKenzie, C. T. Piech, M. Senbetta, K. L. Schulman and E. J. Stepanski, *Support. Care Cancer*, 2012, **20**, 2089–2096.
5 R. K. Jain and T. Stylianopoulos, *Nat. Rev. Clin. Oncol.*, 2010, **7**, 653–664.
6 J. Zhang, B. Shen, L. Chen, L. Chen, Y. Meng and J. Feng, *Colloids Surf., B*, 2019, **175**, 65–72.
7 J. Z. Zhou, X. Ma, R. J. Ju, X. Y. Li, N. Li, M. G. Sun, J. F. Shi, C. X. Zhang and W. L. Lu, *Biomaterials*, 2013, **34**, 3626–3638.
8 S. K. Choi, A. Myc, J. E. Silpe, M. Sumit, P. T. Wong, K. McCarthy, A. M. Desai, T. P. Thomas, A. Kotlyar, M. M. Holl, B. G. Orr and J. R. Baker, Jr, *ACS Nano*, 2013, **7**, 214–228.

9 Q. Hu, Y. Wang, L. Xu, D. Chen and L. Cheng, *Int. J. Nanomed.*, 2020, **15**, 2751–2764.
10 D. W. Wang, X. M. Zhu, S. F. Lee, H. M. Chan, H. W. Li, S. K. Kong, J. C. Yu, C. H. K. Cheng, Y. J. Wang and K. C. Leung, *J. Mater. Chem. B*, 2013, **1**, 2934–2942.
11 X. Du, S. Yin, L. Xu, J. Ma, H. Yu, G. Wang and J. Li, *Carbohydr. Polym.*, 2020, **229**, 115484.
12 M. K. Patel, M. A. Ali, M. Zafaryab, V. V. Agrawal, M. M. Rizvi, Z. A. Ansari, S. G. Ansari and B. D. Malhotra, *Biosens. Bioelectron.*, 2013, **45**, 181–188.
13 T. Yan, J. He, R. Liu, Z. Liu and J. Cheng, *Carbohydr. Polym.*, 2020, **231**, 115706.
14 N. N. Ferreira, S. Granja, F. I. Boni, L. M. B. Ferreira, R. M. Reis, F. Baltazar and M. P. D. Gremiao, *Drug Delivery Transl. Res.*, 2020, **10**, 594–609.
15 R. Sabra, N. Billa and C. J. Roberts, *Int. J. Pharm.*, 2019, **572**, 118775.
16 Z. He, H. Zhu and P. Zhou, *J. Fluoresc.*, 2012, **22**, 193–199.
17 L. Han, L. B. Du, A. Kumar, H. Y. Jia, X. J. Liang, Q. Tian, G. J. Nie and Y. Liu, *Biomaterials*, 2012, **33**, 8517–8528.
18 L. Du, X. Miao, Y. Gao, H. Jia, K. Liu and Y. Liu, *Nanomedicine*, 2014, **10**, 1411–1420.
19 R. Hao, R. Xing, Z. Xu, Y. Hou, S. Gao and S. Sun, *Adv. Mater.*, 2010, **22**, 2729–2742.
20 C. W. Leung, Y. Hong, S. Chen, E. Zhao, J. W. Lam and B. Z. Tang, *J. Am. Chem. Soc.*, 2013, **135**, 62–65.
21 C. Sun, Z. Cao, M. Wu and C. Lu, *Anal. Chem.*, 2014, **86**, 11403–11409.
22 Y. C. H. Wang, G. M. Lin, I. Roy and K. T. Yong, *ACS Appl. Mater. Interfaces*, 2013, **5**, 2786–2799.
23 C. Liu, K. K. Ewert, W. Yao, N. Wang, Y. Li, C. R. Safinya and W. Qiao, *ACS Appl. Mater. Interfaces*, 2020, **12**, 70–85.
24 Q. Zhuang, H. Jia, L. Du, Y. Li, Z. Chen, S. Huang and Y. Liu, *Biosens. Bioelectron.*, 2014, **55**, 76–82.
25 T. Chen, S. Xu, T. Zhao, L. Zhu, D. Wei, Y. Li, H. Zhang and C. Zhao, *ACS Appl. Mater. Interfaces*, 2012, **4**, 5766–5774.
26 H. S. Choi, W. Liu, P. Misra, E. Tanaka, J. P. Zimmer, B. Itty Ipe, M. G. Bawendi and J. V. Frangioni, *Nat. Biotechnol.*, 2007, **25**, 1165–1170.
27 A. Aravind, P. Jeyamohan, R. Nair, S. Veeranarayanan, Y. Nagaoka, Y. Yoshida, T. Maekawa and D. S. Kumar, *Biotechnol. Bioeng.*, 2012, **109**, 2920–2931.
28 S. Soundararajan, L. Wang, V. Sridharan, W. Chen, N. Courtenay-Luck, D. Jones, E. K. Spicer and D. J. Fernandes, *Mol. Pharmacol.*, 2009, **76**, 984–991.
29 Q. Z. Xueling Guo, T. Ji, Y. Zhang, C. Li, Y. Wang, Li Hong, H. Jia, Y. Liu and L. Du, *Carbohydr. Polym.*, 2018, **195**, 311–320.
30 C. T. Chen, W. J. Chen, C. Z. Liu, L. Y. Chang and Y. C. Chen, *Chem. Commun.*, 2009, 7515–7517.
31 P. H. Li, J. Y. Lin, C. T. Chen, W. R. Ciou, P. H. Chan, L. Luo, H. Y. Hsu, E. W. Diau and Y. C. Chen, *Anal. Chem.*, 2012, **84**, 5484–5488.
32 H. Kawasaki, H. Yamamoto, H. Fujimori, R. Arakawa, Y. Iwasaki and M. Inada, *Langmuir*, 2010, **26**, 5926–5933.
33 Q. Ning, Y. F. Liu, P. J. Ye, P. Gao, Z. P. Li, S. Y. Tang, D. X. He, S. S. Tang, H. Wei and C. Y. Yu, *ACS Appl. Mater. Interfaces*, 2019, **11**, 10578–10588.
34 S. K. Hindupur, M. Colombi, S. R. Fuhs, M. S. Matter, Y. Guri, K. Adam, M. Cornu, S. Piscuoglio, C. K. Y. Ng, C. Betz, D. Liko, L. Quagliata, S. Moes, P. Jenoe, L. M. Terracciano, M. H. Heim, T. Hunter and M. N. Hall, *Nature*, 2018, **555**, 678–682.
35 M. Ikeda, C. Morizane, M. Ueno, T. Okusaka, H. Ishii and J. Furuse, *Jpn. J. Clin. Oncol.*, 2018, **48**, 103–114.
36 F. S. Wang, J. G. Fan, Z. Zhang, B. Gao and H. Y. Wang, *Hepatology*, 2014, **60**, 2099–2108.
37 T. Utsunomiya, M. Shimada, Y. Morine, A. Tajima and I. Imoto, *Cancer Sci.*, 2014, **105**, 749–754.
38 R. S. C. M. L. F. De Queiroz Antonino, B. R. P. Lia Fook, V. A. de Oliveira Lima, R. Í. de Farias Rached, E. P. N. Lima, R. J. da Silva Lima, C. A. Peniche Covas and M. V. Lia Fook, *Mar. Drugs*, 2017, **15**, 141.
39 A. D. Bernkop-Schnürch and S. Duennhaupt, *Eur. J. Pharm. Biopharm.*, 2012, **81**, 463–469.
40 Z. L. Kong, H. P. Kuo, A. Johnson, L. C. Wu and K. L. B. Chang, *Int. J. Mol. Sci.*, 2019, **20**, 2918.
41 L. B. Du, S. Suo, D. Luo, H. Y. Jia, Y. L. Sha and Y. Liu, *J. Nanopart. Res.*, 2013, **15**, 1708–1714.
42 A. D. Ellington and J. W. Szostak, *Nature*, 1990, **346**, 818–822.
43 H. G. J. Alqaraghuli, S. Kashanian and R. Rafipour, *Curr. Pharm. Biotechnol.*, 2019, **20**, 1087–1107.
44 A. Barzegar Behrooz, F. Nabavizadeh, J. Adiban, M. Shafiee Ardestani, R. Vahabpour, M. R. Aghasadeghi and H. Sohanaki, *Clin. Exp. Pharmacol. Physiol.*, 2017, **44**, 41–51.
45 L. Li, J. Hou, X. Liu, Y. Guo, Y. Wu, L. Zhang and Z. Yang, *Biomaterials*, 2014, **35**, 3840–3850.
46 Z. Luo, Z. Yan, K. Jin, Q. Pang, T. Jiang, H. Lu, X. Liu, Z. Pang, L. Yu and X. Jiang, *J. Colloid Interface Sci.*, 2017, **490**, 783–796.
47 S. Li, W. Su, H. Wu, T. Yuan, C. Yuan, J. Liu, G. Deng, X. Gao, Z. Chen, Y. Bao, F. Yuan, S. Zhou, H. Tan, Y. Li, X. Li, L. Fan, J. Zhu, A. T. Chen, F. Liu, Y. Zhou, M. Li, X. Zhai and J. Zhou, *Nat. Biomed. Eng.*, 2020, **4**, 704–716.